Chinese Journal of
POLYMER SCIENCE

RESEARCH ARTICLE

https://doi.org/10.1007/s10118-023-3012-5
Chinese J. Polym. Sci. **2023**, *41*, 1617–1628

Remarkably Improved Gas Separation Performance of Polyimides by Forming "Bent and Battered" Main Chain Using Paracyclophane as Building Block

Lu-Jun Huang[a,b], Ya-Tao Weng[a,b], Aqib Raiz[a,b], Zhi-Jie Mao[c*], and Xiao-Hua Ma[a,b*]

[a] *State Key Laboratory of Separation Membranes and Membrane Processes, Tiangong University, Tianjin 300387, China*
[b] *School of Materials Science and Engineering, Tiangong University, Tianjin 300387, China*
[c] *Jiangxi Key Laboratory of Organic Chemistry, Jiangxi Science & Technology Normal University, Nanchang 330013, China*

Electronic Supplementary Information

Abstract The design and development of highly permeable, selective and stable polymer membranes are great challenges in the gas separation industry. Herein, we constructed two intrinsic microporous polyimides (6FPCA and 6FMCA) derived from two isometric diamines (PCA and MCA), which were synthesized by palladium catalyzed C—N coupling reaction. The PCA and MCA diamines contain a hollow beaded structure of 2,2′-paracyclophane as a building block with a specified window size of 3.09 Å. The chemical structures of monomers, polyimides were confirmed by NMR, FTIR, and elementary analysis. 6FPCA and 6FMCA exhibit good solubility, excellent thermal stability, and mechanical properties. 6FPCA exhibits much larger microporosity (434 versus 120 $m^2 \cdot g^{-1}$), FFV (0.22 versus 0.15), *d*-spacing (6.9 versus 5.9 Å), and over 10 times higher permeability with a very little decrease in selectivity than the corresponding polyimide (6FpA) with a plane structure, which remarkably increased their separation performance from far below the 2008 Robeson Upper bounds to reach these limitations for O_2/N_2 and CO_2/CH_4. Additionally, the 6FPCA also demonstrates good plasticization resistance, moderate aging properties, and high CO_2/CH_4 mixed-gas separation performance. These results indicate that paracyclophane subunit can be successfully incorporated into polymers to enhance their ultra-microporosity and separation properties, which open a new avenue for developing high performance gas separation membranes with topological ultra-micropores.

Keywords Polyimide of intrinsic microporosity; 2,2′-Paracyclophane; Molecular intrinsic microporosity; Gas separation; Permeability/selectivity trade-off

Citation: Huang, L. J.; Weng, Y. T.; Raiz, A.; Mao, Z. J.; Ma, X. H. Remarkably improved gas separation performance of polyimides by forming "bent and battered" main chain using paracyclophane as building block. *Chinese J. Polym. Sci.* **2023**, *41*, 1617–1628.

INTRODUCTION

Membrane technology is considered as one of the most promising methods to realize carbon neutralization due to its versatile advantages such as small footprint, less energy-intensive, no phase change during separation, easy operation and modules.[1,2] The membranes play a crucial role in this technique, and as a result, advanced membranes with high permeability, selectivity and durability simultaneously are in great desire.[3–6] However, the permeability/selectivity relationship of the membranes is restricted by a trade-off effect; that is, for a specific membrane, the high permeability always results in a low selectivity and *vice versa*, which makes the development of high performance gas separation membranes a great challenge.[7–10]

Till now, creating some sub-nanometer channels to transport gases by molecular sieving effect is recognized as the most efficient method to realize both high permeable and selective gas separation membranes.[11–13] One efficient strategy is to form polymers of intrinsic microporosity (PIMs), the origin of sieving properties in these PIMs is the site of contortions in their repeat unit that cannot form closed packing in the condensed state, thus resulting in a large amount of micropore (2 nm) or ultra-micropore (<0.7 nm) in the range of the dynamic diameters of gas molecules (2.9 Å to 3.84 Å), and consequently, polymer molecular sieves are formed with strong selectively transport gases.[14–17] This was realized by the state-of-the-art PIM-1 in 2004, and after that, rapid development of PIMs was observed by changing the contortion centers and shape persistent chemical structures of polymer main chain.[18–23] Some newly reported PIMs even pushed forward the trade-off curves from 2008 to 2015 for O_2/N_2 and H_2/N_2, and 2019 for CO_2/N_2 and CO_2/CH_4 gas pairs.[7,8,10] Among these PIMs, the "kinked" structures, ranging from

* Corresponding authors, E-mail: mzjnju@jxstnu.edu.cn (Z.J.M.)
E-mail: xhuama@tiangong.edu.cn (X.H.M.)

Special Issue: Celebrating the 70th Anniversary of the Establishment of Polymer Program at Peking University
Received April 19, 2023; Accepted May 28, 2023; Published online July 5, 2023

spirobisindane, spirobifluorene, triptycene, Tröger's base, CANAL subunits and their derivatives, play an important role in their gas separation properties,[20,22,24–34] additionally, the rigidity and symmetry induced more ultra-micropore during their chain packing in the condensed state further enhanced their separation properties.

Unlike PIMs that form micropores by inefficient chain packing in the solid states, another kind of novel PIM was formed using supramolecular structures with specified sieving topological pores that emerged recently. For example, the Chung' s group incorporated the cyclodextrin (CD) structure into PIM-1 and formed PIM-CD membrane, which demonstrated improved permeability, selectivity, and aging resistance than PIM-1.[35,36] At the same time, modified CD, sulfothiacalix macrocycle structures have also been used for efficient organic nanofiltration applications because they have a certain size-distributing macrocycle structure,[37–42] which significantly enhanced their flux and stability even under harsh conditions. This is because the ultra-micropores in these polymers are formed by topological void and very stable, which is different from those unstable pores of PIMs that are in an intermediate state with strong physical aging.[36]

2,2-Paracyclophane is a "bent and battered" site of contortion (Fig. 1) formed by Winberg dimerization reaction.[43] It is an important scaffold in asymmetric synthesis, energy, and functional coatings materials with broad applications in bio- and materials science.[44–47] In which, the two aromatic rings are connected with two ethylene bridges at 1,1′ and 4,4′ positions. Thus, a molecular ultra-micropore with a window size of 3.09 Å is formed (Fig. 1),[44] which belongs to the ultra-micropore region and close to the dynamic diameters of these gas molecules, and consequently, has good potential for gas separation membranes.[48]

To take advantage of the stable topological molecular ultra-micropore of 2,2′-paracyclophane, we designed two intrinsic microporous polyimides by reacting with 4,4'-(hexafluoroisopropylidene)diphthalic anhydride (6FDA) with 2,2′-paracyclophane-4,16-diamine (PCA, pseudo *para* substitution) and 2,2′-paracyclophane-4,15-diamine (MCA, pseudo *meta* substitution). For better comparison, two polyimides with plane structures were also synthesized by the condensation reaction of 6FDA with *para* phenylene diamine (pA) and meta phenylenediamine (mA) (Fig. 1). The structures, thermal, chemical, mechanical and microporosity properties of these polyimides were fully characterized, their gas transport properties including the permeability, pure- and mixed-gas selectivity, pressure-dependent and thermal dynamics gas transport are also analyzed in detail to elucidate the effect of this paracyclophane topological ultra-micropore effect.

EXPERIMENTAL

Materials and Characterizations

2,2′-Paracyclophane, tetrachloromethane (CCl_4), bromine (Br_2), sodium t-butoxide, 2,2′-bis(diphenylphosphino)-1,1′-binaphthyl (BINAP), benzophenone imine, toluene, tetrahydrofuran, tris(dibenzylideneacetone)dipalladium ($Pd_2(dba)_3$), sodium hydroxide, dichloromethane, 4,4'-(hexafluoroisopropylidene) diphthalic anhydride (6FDA), *meta* phenylenediamine (mA), paraphenylenediamine (pA), 1,4-dioxane, hydrochloric acid, and trichloromethane were obtained from J&K and used as received.

Synthesis of the Monomers

The synthesis scheme of the monomers is shown in Scheme 1, and the details are described as follows.

Synthesis of PCA and MCA monomers

4,15(16)-Dibromoparacyclophane. 2,2′-Paracyclophane (21.5 g, 0.104 mmol) and CCl_4 (300 mL) were added to a 500 mL three-

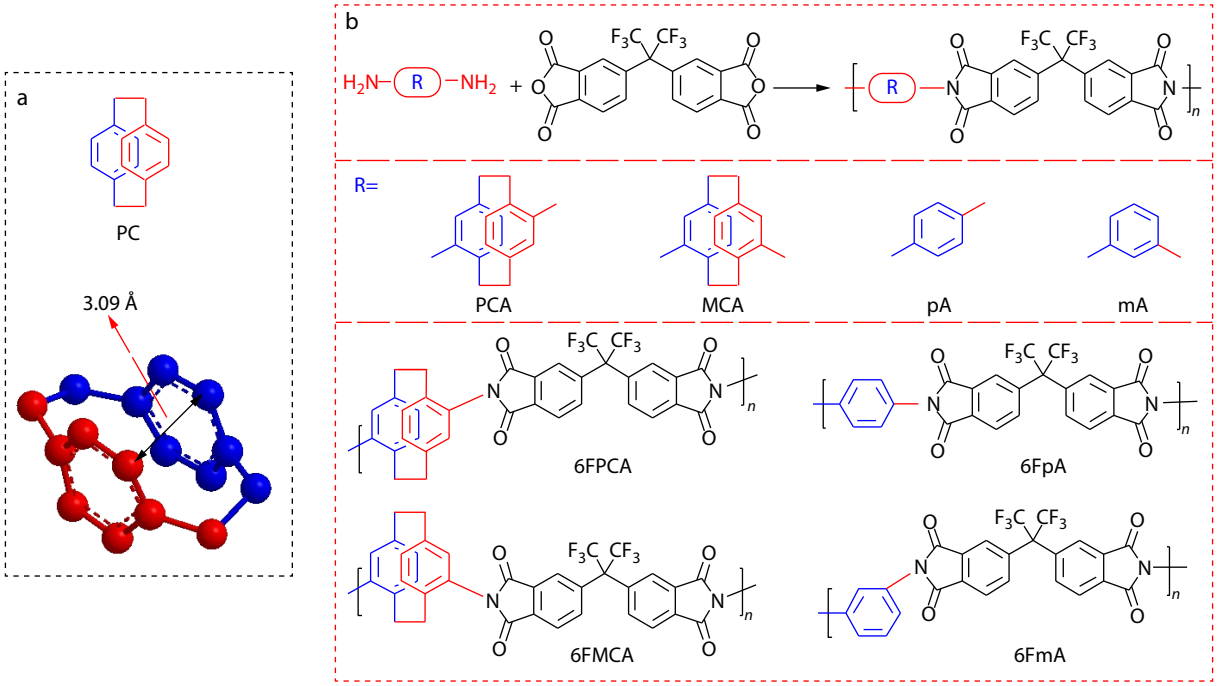

Fig. 1 (a) Chemical and 3D structure of 2,2′-paracyclophane molecule, the distance between the benzene rings (3.09 Å) is highlighted; (b) Synthetic procedures of the 6FPCA, 6FMCA, 6FpA, and 6FmA polyimides.

https://doi.org/10.1007/s10118-023-3012-5

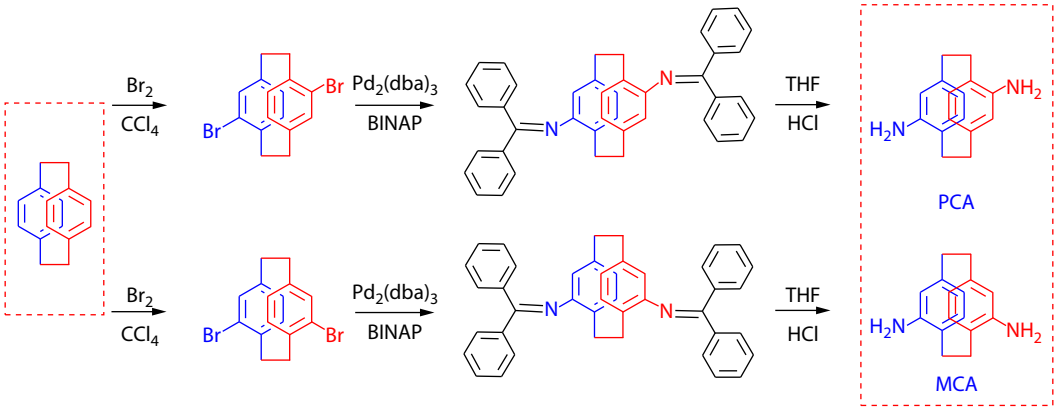

Scheme 1 Synthetic procedures of PCA and MCA monomers.

necked round-bottomed flask, which was heated to 55 °C and then stirred for 30 min. After that, a solution of Br_2 (99.5 g, 0.620 mmol) in CCl_4 (30 mL) was added dropwisely. The thin layer chromatography (TLC) results indicated that the reaction was finished in 2 h. The solution was then poured into water (1000 mL), and a colorless solution was formed after washing with $Na_2S_2O_3$ (aq.). The organic phase was dried with $MgSO_4$, most of the solvent was removed by a rota-evaporator and a large amount of solid was precipitated, which was washed with hot ethanol and hexane in sequence. The remaining solid was then washed with chloroform for twice, and the undissolved solid was re-crystallized in 1,4-dioxane twice; the neat 4,16- dibromo-paracyclophane (in the pseudo *para* position) can be obtained at a 35% yield. The mother solvent of chloroform was removed by a rota-evaporator, which was further re-crystallized by ethanol, and the 4,15-dibromo-paracyclophane (in the pseudo *meta* position) can be obtained in a 40% yield.

PCA. 4,16-Dibromoparacyclophene (20.6 g, 56.2 mmol), sodium ter-butoxide (13.2 g, 137 mmol), $Pd_2(dba)_3$ (0.521 g, 0.569 mmol), BINAP (0.944 g, 1.52 mmol), benzophenone imine (24.4 g, 135 mmol) and toluene (350 mL) were added in sequence to a 500 mL three-necked round-bottomed flask under Ar atmosphere. The system was cooled in liquid nitrogen for 0.5 h, then vacuumed by a pump and refilled with Ar for three times to exchange the O_2 inside fully. The reaction was then heated to reflux for 14 h, followed by cooling to r.t. The precipitate was collected by filtration. After washing with toluene, the solid was dissolved in 200 mL of THF in a 500 mL flask, HCl (200 mL, 1 N) was added, and the reaction was refluxed for 4 h, cooled to room temperature and then neutralized with NaOH solution (1 mol/L). The aqueous phase was extracted with dichloromethane three times (3×150 mL). The organic phase was collected and dried with $MgSO_4$, the solvent was removed, an off-white solid was obtained, which was then loaded onto a column, and the pure product of PCA (8.40 g, yield: 63%) could be obtained. ^{1}H-NMR (400 MHz, DMSO-d_6, δ, ppm): 6.31–6.33 (m, 2H), 5.98–6.00 (m, 2H), 5.32 (s, 2H), 4.50 (s, 4H), 3.13–3.19 (m, 2H), 2.85–2.92 (m, 2H), 2.61–2.66 (m, 2H), 2.37–2.44 (m, 2H); ^{13}C-NMR (100 MHz, $CDCl_3$, δ, ppm): 147.2, 139.9, 134.1, 122.5, 121.7, 119.0, 32.8, 31.6. HRMS for $C_{16}H_{18}N_2$, Calcd. For 238.1470, Found for 238.1548.

MCA. The synthesis and purification of MCA were the same procedure as that of PCA, with a yield is 60%. ^{1}H-NMR (400 MHz, DMSO-d_6, δ, ppm): 6.76–6.78 (m, 2H), 5.72–5.75 (m, 2H), 5.33 (s, 2H), 4.43 (s, 4H), 2.84–2.92 (m, 2H), 2.68–2.75 (m, 2H), 2.63–2.64 (m, 4H); ^{13}C-NMR (100 MHz, $CDCl_3$, δ, ppm): 147.8, 139.4, 128.5, 123.0, 120.5, 119.9, 34.9, 29.3. HRMS for $C_{16}H_{18}N_2$, Calcd. for 238.1470, Found for 238.1551.

Synthesis of the 6FPCA, 6FMCA, 6FpA and 6FmA polyimides

6FPCA. 6FDA (2.22 g, 5.00 mmol), PCA (1.19 g, 5.00 mmol) and *m*-cresol (17.0 mL) were added to a 100 mL single-necked flask under Ar atmosphere, which was stirred for 0.5 h till all reagents were dissolved before isoquinoline was added. The solution was gradually heated to 180 °C and kept for 2 h. A very high viscous solution was formed, which was then cooled to ~50 °C and poured into methanol (300 mL). The yellow fibrous polymer was precipitated, which was dried in a blastic oven at 80 °C, and then repeatedly dissolved in $CHCl_3$ and precipitated in methanol twice. The neat 6FPCA polymide (2.87 g, yield: 89%) was obtained after drying in an oven at 80 °C for 12 h till constant weight. ^{1}H-NMR (400 MHz, $CDCl_3$, δ, ppm): 8.12 (s, 2H), 8.03 (s, 2H), 7.95 (s, 2H), 6.89 (s, 2H), 6.87 (s, 4H), 6.51 (s, 2H), 3.19 (s, 4H), 2.93 (s, 4H). FTIR (wavenumber, cm^{-1}): 2930 (CH_2 vibration stretching), 1785 (C=O, asymmetric stretching), 1720 (C=O, symmetric stretching), 1355 (C—N, stretching). Anal. for $C_{35}H_{20}F_6N_2O_4$: Calcd. for: C, 65.0; H, 3.10; N, 4.33; Found: C, 64.3; H, 3.12; N, 4.37; T_d = 508 °C (T_d represents the onset decomposition temperature), S_{BET}=434 $m^2 \cdot g^{-1}$.

6FMCA. The synthetic procedure of 6FMCA was the same as that of 6FPCA; the product was obtained as a yellow solid with a yield of 91%. ^{1}H-NMR (400 MHz, $CDCl_3$, δ, ppm): 8.11 (s, 2H), 7.99 (s, 2H), 7.91 (s, 2H), 6.89 (s, 2H), 6.81 (s, 4H), 6.51 (s, 2H), 3.26 (s, 2H), 3.10 (s, 4H), 2.71 (s, 2H). FTIR (wavenumber, cm^{-1}): 2930 (CH_2 stretching vibration), 1785 (C=O, asymmetric stretching), 1720 (C=O, symmetric stretching), 1355 (C—N, stretching). Anal. for $C_{35}H_{20}F_6N_2O_4$: Calcd. for: C, 65.0; H, 3.10; N, 4.33; Found: C, 64.5; H, 3.08; N, 4.31. T_d=508 °C, S_{BET}=420 $m^2 \cdot g^{-1}$.

6FpA. 6FDA (3.33 g, 7.50 mmol), pA (0.810 g, 7.50 mmol) and *m*-cresol (16.5 mL) was added to a 100 mL three necked flask under Ar flow, and the reaction was continuously stirred at room temperature to get a clear solution. Isoquinoline (1.0 mL) was added, and the reaction system was gradually increased to 180 °C and kept for 2 h. After cooling to room temperature, the solution was poured into methanol (300 mL), dried in the air, re-dissolved in DMF and precipitated in methanol to get a light yellow fibrous polymer. The remaining DMF was removed using a Soxhlet extraction by methanol for 10 h. A yellow filament was obtained (3.48 g, 90% yield) after drying in an oven at 80 °C for 12 h. ^{1}H-NMR (400 MHz, DMSO-d_6, δ, ppm): 8.20 (s, 1H), 8.18 (s,

https://doi.org/10.1007/s10118-023-3012-5

1H), 7.97 (s,1H), 7.95 (s, 1H), 7.77 (s, 2H), 7.57 (s, 2H), 7.55 (s, 2H). FTIR (wavenumber, cm^{-1}): 1785 (C=O, asymmetric stretching), 1720 (C=O, symmetric stretching), 1355 (C—N, stretching vibration). Anal. For: $C_{25}H_{10}F_6N_2O_4$; Calcd. for: C, 58.1; H, 1.94; N, 5.43; Found: C, 57.5; H, 1.96; N, 5.39. GPC: M_n=72.1 kDa, PDI=1.7, T_d=529 °C, S_{BET}=126 $m^2 \cdot g^{-1}$.

6FmA. The synthesis and process of 6FmA was the same as that of 6FpA with a yield of 88%. ^{1}H-NMR (400 MHz, DMSO-d_6, δ, ppm): 8.25 (s, 1H), 8.23 (s, 1H), 8.02 (s,1H), 8.00 (s, 1H), 7.79 (s, 2H), 7.63 (s, 4H). FTIR (wavenumber, cm^{-1}): 1785 (C=O, asymmetric stretching), 1720 (C=O, asymmetric stretching), 1355 (C—N, stretching vibration). Anal. for: $C_{25}H_{10}F_6N_2O_4$; Calcd. for: C, 58.1; H, 1.94; N, 5.43; Found: C, 64.3; H, 3.12; N, 4.37. GPC: M_n=98.7 kDa, PDI=1.6, T_d=528 °C, S_{BET}=97 $m^2 \cdot g^{-1}$.

Membrane Formation

Preparation of 6FPCA and 6FMCA membranes

6FPCA and 6FMCA polyimide powders were dissolved in chloroform at a concentration of 2%, which was filtrated into a glass petri dish using a PTFE filter with an average pore size of 0.45 μm. The solvent volatilization was controlled to finish in 24 h. 6FPCA and 6FMCA films with an average thickness of 70 μm were obtained, which were soaked in methanol for 10 h and further dried in a vacuum oven at 120 °C for 4 h before testing. The total removal of the solvent was confirmed by TGA testing.

Preparation of 6FpA and 6FmA membranes

6FpA and 6FmA polyimide powders were dissolved in DMF at a concentration of 2%. The solution was then filtered into a 60 mm petri dish through a hydrophobic PTFE filter with a pore size of ~0.45 μm. The solution was controlled to evaporate in a blastic oven at 85 °C for 24 h, and the prototype 6FpA and 6FmA films can be obtained. The 6FpA and 6FmA membranes were then loaded into a tube furnace and heated to 180 °C under Ar atmosphere for 2 h to totally remove the tiny remaining DMF, which was also proved by TGA testing.

Gas Permeation Measurement

Pure-gas, mixed-gas and the pressure/temperature related gas permeation testing of the 6FPCA, 6FMCA, 6FpA and 6FmA membranes were carried out according to our previous work[49] and shown in the electronic supplementary information (ESI).

RESULTS AND DISCUSSION

Synthesis and Characterization of the Monomers and Polyimides

The following steps can obtain the paracyclophene-based diamine regioisomer monomers. First, the Br_2 reacted with 2,2-paracyclophane by electrophilic reaction following the previous step,[50] and the two dibromine substituted 4,16-dibromo-paracyclophane (pPDB) and 4,15-dibromo-paracyclophane (mPDB) can be obtained simultaneously. Although they are mixtures during the reaction, neat pPDB and mPDB can be obtained by washing and repeated recrystallization due to their solubility differences (details are shown in the experimental part). The resulting pPDB and mPDB were then reacted with benzophenone imine to get the diimine-protected paracyclophane *via* the C—N coupling reaction under the catalyst of $Pd_2(dba)_3$ and BINAP as ligand,[51] and the crude product can be used directly to the next hydrolysis step, and the PCA and MCA monomers can be obtained by column chromatography, the overall yield of the two steps was reasonable to be ~63%. The structure and purity of the PCA and MCA diamine isomer monomers were confirmed by the NMR, FTIR and HRMS characterizations. The NMR spectra are shown in Fig. 2, in which the chemical shift of proton at 4.50 ppm confirms the diamines of the two monomers. Because the PCA is a C_i symmetry and the MCA shows a C_2 symmetry, which causes distinct chemical shifts of the protons in the aromatic and the bridge part. For example, the PCA exhibited a higher shielding effect on aromatic proton "**a**" than MCA (6.31 versus 6.77 ppm, Fig. 2a); at the same time, it also shows 4 different types of methylene protons (**e**, **f** and **h**, between 2.2 and 3.2 ppm), whereas the MCA only exhibits three types of methylene protons, which is due to the stereo effect (endo and exo) of the protons in the $-CH_2-$ groups that cannot rotate freely. Aside from their ^{1}H-NMR spectra, the chemical shift differences of the carbons in their ^{13}C-NMR are more pronounced, especially in the aliphatic part (Fig. 2b). Due to the diamines in MCA are point to the same direction, the chemical shift differences of the two

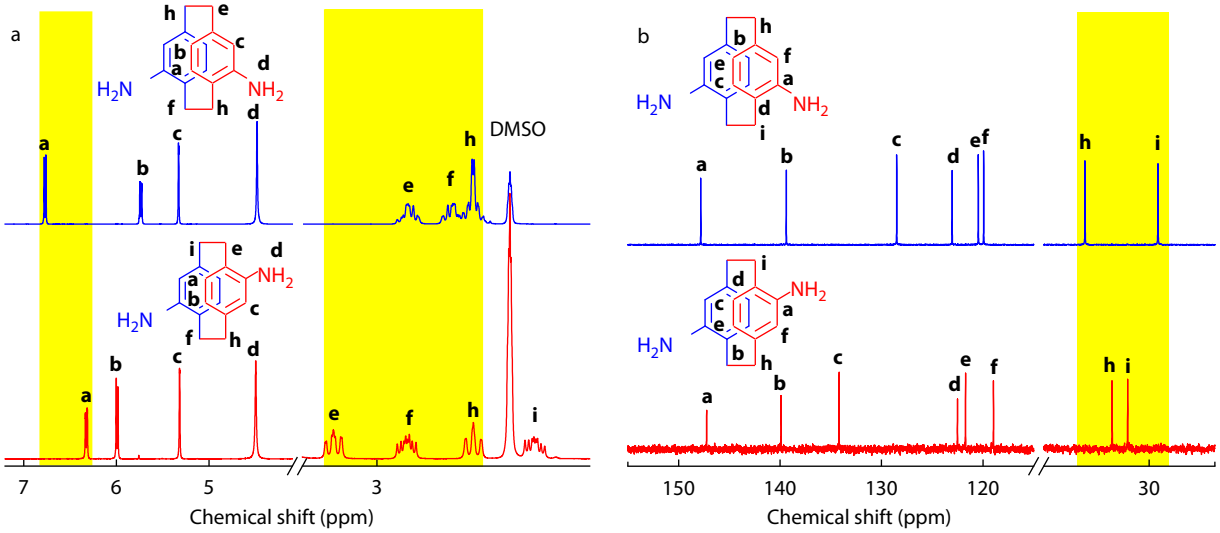

Fig. 2 (a) ^{1}H-NMR and (b) ^{13} C-NMR spectra of PCA and MCA monomers.

https://doi.org/10.1007/s10118-023-3012-5

—CH_2— carbons (**h** and **i**) in MCA (34.9 and 29.3 ppm) are much larger than that of PCA (32.8 and 31.6 ppm, Fig. 2b).

When reacting the PCA, MCA, pA and mA with 6FDA, four polyimides (6FPCA, 6FMCA, 6FpA and 6FmA) can be synthesized using *m*-cresol as solvent and isoquinoline as a catalyst. Their chemical structures and ^{1}H-NMR spectra are shown in Fig. 3.

The protons of 6FDA part are shown in the range of 7.9–8.3 ppm, and the rest protons belong to the PCA or MCA, which confirms the successfully synthesis of the two polyimides. Due to the topological differences of the PCA and MCA monomers, there are huge variations in the 6FPCA and 6FMCA polyimides, *i.e.*, the 6FPCA exhibits two types of aliphatic protons at 3.19 and 2.93 ppm, whereas the 6FMCA demonstrated three distinct —CH_2— peaks ranging from 3.26, 3.10, and 2.71 ppm. Additionally, the aromatic protons of **d** and **e** in 6FMCA exhibited a big shoulder (ranging from 6.5 ppm to 7.0 ppm), while in 6FPCA, they are almost immerged with each other.

The structures of the two paracyclophane-based polyimides are also confirmed by their FTIR spectra (Fig. S1 in ESI). They exhibit not only conventional imide signals at the wavenumbers of 1785, 1720, and 1355 cm^{-1},[52] but also demonstrate the stretching vibration bands of —CH_2— at 2930 cm^{-1}, which can not be observed in 6FpA and 6FmA (Fig. S1 in ESI). All polyimides show moderate solubility in conventional solvents (Table S1 in ESI), in which the 6FPCA and 6FMCA with paracyclophane subunit increased the solubility in halide substituted solvents such as chloroform and dichloromethane, whereas decreased the solubility in high polar aprotic solvents such as DMF and DMAc. Consequently, chloroform was chosen for membrane formation of 6FPCA, 6FMCA, and DMF was selected for 6FpA and 6FmA. The details are described in the experimental part.

Thermal and Mechanical Properties of 6FPCA, 6FMCA, 6FpA and 6FmA Membranes

All polyimides show excellent thermal stabilities, as confirmed by their TGA curves (Fig. S2 and Table S2 in ESI). Interestingly, the 6FPCA and 6FMCA have almost identical TGA curves, a similar phenomenon can be observed in 6FpA and 6FmA. The 6FPCA demonstrates a slightly lower onset decomposition temperature (T_d) than 6FpA (508 versus 529 °C, Table S2 in ESI), which is attributed to the methylene group that reduces the thermal stability of the resulting polyimide. All polyimides show high glass transition temperatures as indicated by their DMA curves, that is, 6FPCA (398 °C), 6FpA (380 °C), 6FMCA (354 °C), and 6FmA (310 °C). The PIs with paracyclophane exhibit a higher T_g than the PI without this building block, *i.e.*, 6FMCA showed a 44 °C higher T_g than 6FmA, indicating the incorporation of the paracyclophane subunit enhanced the rigidity of the polymer main chain. At the same time, the diamines in the para-position substitution demonstrated much higher T_g than that in the meta ones (Table S2 in ESI), which may attribute to the diamines at the *meta*-position are more flexible than the *para*-substituted diamine and tend to arrange in a closer packing.[53]

All polyimide membranes have good mechanical properties, and their stress-strain curves are shown in Fig. 4. The 6FpA and 6FmA show a strength of ~85 MPa combined with Young's Modulus of 1.68–2.04 GPa (Table S3 in ESI). This value is quite high among those reported polyimides used in gas separations.[30] The 6FPCA and 6FMCA demonstrated a lower mechanical strength (68–77 MPa) and Young's modulus (1.43–1.45 GPa) than 6FpA and 6FmA, this may originate from the stronger π-π interaction and more compact packing of 6FpA and 6FmA that enhances the chain-chain interaction, whereas in the 6FPCA and 6FMCA, which is interrupted in the four —CH_2— groups in the paracyclophane subunit.

WAXD and Microporosity of 6FPCA, 6FMCA, 6FpA and 6FmA Membranes

To analyze the effect of introducing paracyclophane subunit on the chain packing of the resulting polyimide membranes, their WAXD spectra were carried out and shown in Fig. 5.

All polyimide membranes demonstrate amorphous structures as indicated by their big halos from ~10° to 30°. After deconvolution, these peaks can be subdivided into two or three peaks, there is a main halo at ~10° to 20° and a relatively small halo ~20° to 30°. The two diamines with plane structures derived 6FpA and 6FmA show a more compact packing, *e.g.*, the 6FpA shows *d*-spacings derived from their diffraction peaks by Bragg's law are 5.90, 4.19 and 3.29 Å, re-

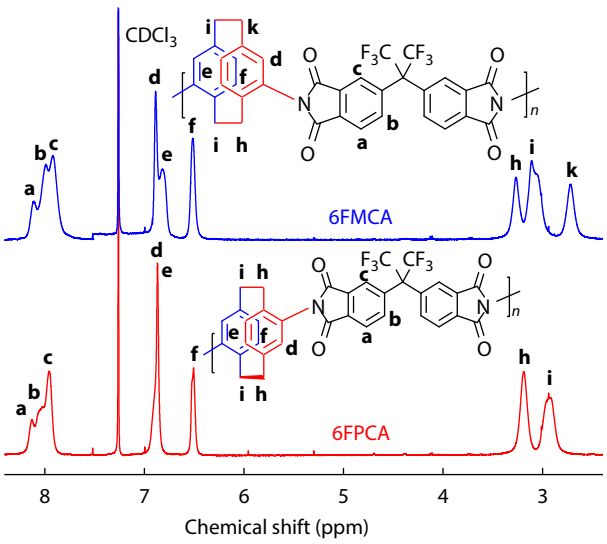

Fig. 3 ^{1}H-NMR spectra of 6FPCA and 6FMCA.

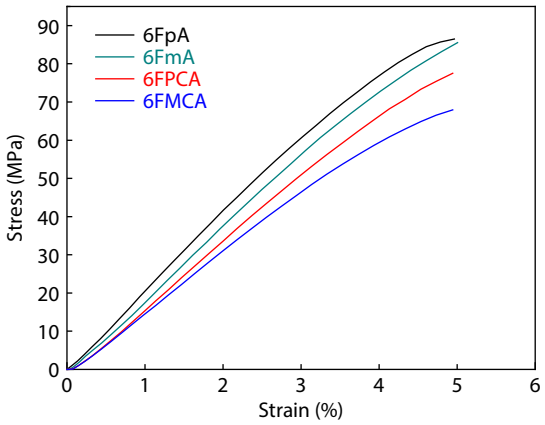

Fig. 4 Stress-strain curves of 6FPCA, 6FMCA, 6FpA and 6FmA membranes.

https://doi.org/10.1007/s10118-023-3012-5

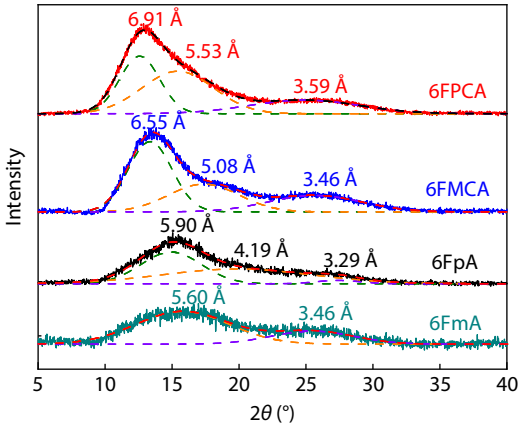

Fig. 5 Wide angle X-ray diffraction (WAXD) patterns of 6FPCA, 6FMCA, 6FpA and 6FmA membranes with a thickness of ~60 μm.

spectively, which is smaller than the 6FPCA with the *d*-spacing of 6.91, 5.53 and 3.59 Å. Compared with 6FPCA and 6FMCA, the *para*-substituted paracyclophane gives a more open structure than the *meta*-substituted counterpart, with their *d*-spacings, are 6.91 versus 6.55, 5.53 versus 5.08, and 3.59 versus 3.64 Å, respectively. This is probably due to the C_2 symmetry of MCA tends to form a more compact structure than the C_i symmetry of PCA in their chain packing. Similar trends can also be observed in 6FpA and 6FmA membranes.[53]

The N_2 adsorption/desorption isotherms of these polyimides at −196 °C are shown in Fig. 6. Both 6FPCA and 6FMCA demonstrated type II adsorption behavior as confirmed by the large adsorption at the very low relative pressure (P/P_0<10^{-5}), which proves the microporosity of the resulting polyimides.

The introduction of the paracyclophane subunit significantly enhanced their microporosity, *i.e.*, the BET surface areas increased remarkably from 126 $m^2 \cdot g^{-1}$ (6FpA) to 434 $m^2 \cdot g^{-1}$ (6FPCA) (Table S1 in ESI). Meanwhile, the BET surface area differences of 6FPCA and 6FMCA are very small, that is, 434 and 420 $m^2 \cdot g^{-1}$, respectively. Although lower than those super high PIMs, such as PIM-1 (760 $m^2 \cdot g^{-1}$),[54] PIM-PI-8 (830 $m^2 \cdot g^{-1}$)[18] and KAUST-PI-1 (752 $m^2 \cdot g^{-1}$),[30] these values are

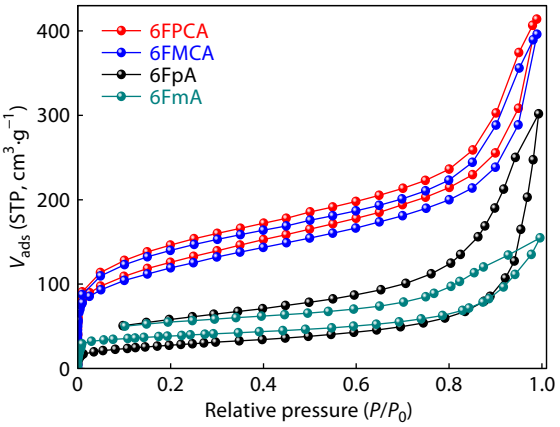

Fig. 6 N_2 adsorption/desorption isotherms of 6FPCA, 6FMCA, 6FpA and 6FmA membranes.

much larger than those of PIM-PIs previously reported such as 6FDA-DAT1 (320 $m^2 \cdot g^{-1}$),[55] CTPI (193 $m^2 \cdot g^{-1}$)[56] and PIM-6FDA-OH (225 $m^2 \cdot g^{-1}$).[57] Notably, the microporosity sequence of these polyimides is the same as their WAXD result; the paracyclophane and its substitution position have a huge effect on the chain packing and microporosity of the resulting membranes.

The density of the polyimides is shown in Table S1 (in ESI), which is reciprocal to their BET surface areas, *e.g.*, the density of the polyimides is 6FPCA<6FMCA<6FpA<6FmA. At the same time, there is an abrupt density decrease when the paracyclophene subunit was introduced, *i.e.*, the densities of 6FpA and 6FmA are 1.487 and 1.513 $g \cdot cm^{-3}$, whereas for 6FPCA and 6FMCA, the values are 1.261 and 1.265 $g \cdot cm^{-3}$, respectively. Their fractional free volumes (FFV) can be calculated using the group contribution theory accordingly.[58] The diamine at the *para* position has a relatively larger FFV than the *meta* position. Meanwhile, there is a sharp increase in the FFV when the paracyclophane is introduced, from ~0.15 to 0.22 (Table S1 in ESI), which is attributed to the more open structures caused by the paracyclophane structure.

Pure-gas Transport Properties

The gas separation properties of the pristine polyimide membranes were measured by the constant volume/variable pressure method. The results and some related polymer membranes are summarized in Table 1. The permeability and selectivity of 6FmA are the same as previous report.[59] The ratio of P_{H_2} over P_{CO_2} decreased from over 3 of 6FmA to less than 1.2 of 6FMCA, indicating the introduction of paracyclophane induced higher FFV that facilitates the transport of CO_2 more than H_2. The permeability sequence of these polyimides is 6FPCA>6FMCA>6FpA>6FmA, which is the same as their *d*-spacing, FFV, and BET surface area.

The polyimides with *para* position substitution (6FPCA and 6FpA) show higher permeability than their corresponding polyimides at *meta* position (6FMCA and 6FmA), which is similar to the previously reported results.[53,64] At the same time, after introducing the paracyclophane subunit, the CO_2 permeability of 6FPCA and 6FMCA significantly increased 16.8 and 48.4 times from their corresponding 6FpA and 6FmA, *i.e.*, from 18.9 Barrer to 320 Barrer and 6.49 Barrer to 314 Barrer, respectively. At the same time, the CO_2/CH_4 selectivity for 6FPCA is 35.6, considering its P_{CO_2} of 320 Barrer, this combination is quite high among those reported high performance CO_2/CH_4 separation PIM-PI membranes such as PIM-6FDA-OH (263 Barrer, CO_2/CH_4=29), 6FDA-DAT1-OH (70 Barrer, CO_2/CH_4=37.5),[65] SBF-HSBF (100 Barrer, CO_2/CH_4 = 41.7), 6FDA-SBF (180 Barrer, CO_2/CH_4=28.4) (Table 1).

Although huge improved permeability, the O_2/N_2, CO_2/CH_4 and CO_2/N_2 selectivity for the 6FPCA and 6FMCA decreased very slightly, *i.e.*, the P_{CO_2} of 6FPCA is 17-fold higher than 6FpA (61.5 versus 3.61 Barrer), whereas their O_2/N_2 selectivities are 4.52 and 5.03, respectively. Consequently, the overall separation performance of the 6FPCA and 6FMCA membranes remarkably increased when compared with the pristine 6FpA and 6FmA, which is proved in their trade-off curves for CO_2/CH_4 and O_2/N_2 (Fig. 7). 6FPCA and 6FMCA show CO_2/CH_4 separation performance on the 2008 trade-off line whereas their corresponding 6FpA and 6FmA falls far below this curve. This result proved that introducing a paracyc-

https://doi.org/10.1007/s10118-023-3012-5

Table 1 Gas permeability and ideal selectivity of 6FPCA, 6FMCA, 6FpA, and 6FmA and some related polymer membranes.

Polymers	Permeability (Barrer)					Ideal selectivity ($a_{x/y}$)		
	H_2	N_2	O_2	CH_4	CO_2	P_{O_2}/P_{N_2}	P_{CO_2}/P_{CH_4}	P_{CO_2}/P_{N_2}
6FPCA [a]	386	13.6	61.5	8.99	320	4.52	35.6	23.5
σ (±)	7.72	0.22	1.61	0.21	8.2	0.08	0.82	0.38
Aged 30 days	309	9.53	46.5	6.42	264	4.88	41.1	27.7
Aged 60 days	295	8.68	43.6	5.54	246	5.02	44.4	28.3
6FMCA [a]	359	12.8	58.8	8.75	314	4.59	35.9	24.5
σ (±)	6.67	0.18	2.01	0.16	7.8	0.06	0.74	0.41
Aged 60 days	308	9.09	46.1	5.69	251	5.07	44.1	27.6
6FpA [b]	33.8	0.718	3.61	0.40	18.9	5.03	47.8	26.3
σ (±)	0.51	0.02	0.13	0.01	0.41	0.11	1.05	0.69
Aged 60 days	26.9	0.55	2.95	0.25	15.8	5.36	63.2	28.7
6FmA [b]	20.0	0.338	1.63	0.171	6.49	4.82	38.0	19.2
σ (±)	0.43	0.01	0.02	0.004	0.16	0.12	1.29	0.41
6FDA-DAP [c]	38	0.37	2.5	0.12	11	6.76	91.7	29.7
6FDA-DAR [c]	34	0.28	1.9	0.09	8	6.79	94.1	28.6
6FDA-SBF [d]	234	7.8	35.1	6.4	182	4.50	28.4	23.3
6FDA-HSBF[d]	162	3.8	19.3	2.4	100	5.08	41.7	26.3
6FDA-DAT1 [e]	198	4.7	25.4	3.2	120	5.40	37.5	25.5
6FDA-PPDA [f]	131	3.2	17	2.5	73	5.31	29.2	22.8
6FDA-APAF [g]	42.8	0.55	3.73	0.21	17.0	6.78	81.0	30.9
PIM-6FDA-OH [h]	259	10.8	45.2	9.1	263	4.2	29	24.0

[a] 6FPCA and 6FMCA membranes with thickness of ~60 μm, soaked in MeOH for 10 h and then dried in a vacuum oven at 120 °C for 4 h; [b] 6FpA and 6FmA membranes with thickness of ~60 μm, dried at 120 °C in vacuum for 2 h; [c] Data from Ref. [60]; [d] Data from Ref. [61]; [e] Data from Ref. [55]; [f] Data from Ref. [62]; [g] Data from Ref. [63]; [h] Data from Ref. [57].

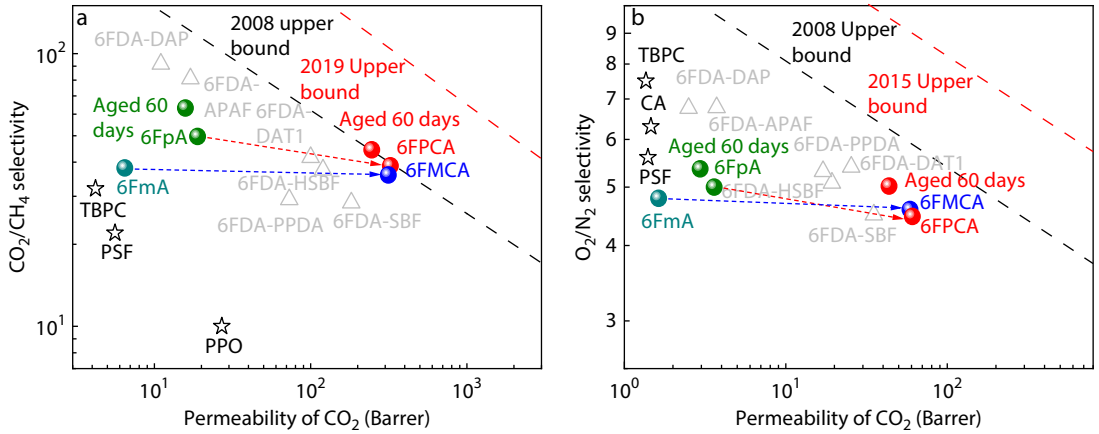

Fig. 7 (a) CO_2/CH_4 and (b) O_2/N_2 separation performance of 6FPCA, 6FMCA, 6FpA, 6FmA and some selected polymers for comparison.

lophane subunit with inner-size sieving pores is very efficient.

Diffusion Solubility Properties of the Membranes

To better understand the effect of introducing paracyclophane on the gas transport behavior of the resulting membranes, the diffusion coefficient (D), and solubility coefficient (S) of N_2, O_2, CH_4 and CO_2, as well as diffusion selectivity (a_D), and solubility selectivity (a_S) of O_2/N_2 and CO_2/CH_4 for these membranes were also obtained (Table 2). After the incorporation of paracyclophane structure, the 6FPCA and 6FMCA demonstrated a much higher D and S than their corresponding 6FpA and 6FmA. For example, the D for N_2 increased 11.6 times from 0.597×10^{-8} $cm^2\cdot s^{-1}$ of 6FpA to 6FPCA of 6.92×10^{-8} $cm^2\cdot s^{-1}$, their S improved only 1.6 times from 1.20×10^{-2} $cm^3\cdot cm^{-3}\cdot cmHg^{-1}$ to 1.97×10^{-2} $cm^3\cdot cm^{-3}\cdot cmHg^{-1}$, which indicates that the permeability increase of the 6FPCA is major comes from the enhancement of D.

Physical Aging Properties of the Membranes

Physical aging of the membranes is very important concerning their practical applications.[66,67] Herein, the 30 and 60 days aging for certain polyimides are tested, and the results are shown in Table 1. Decreased permeability combined with slightly enhanced gas pair selectivity as the aging time increased was observed. 6FPCA shows an 18% CO_2 permeability decrease in the first 30 days, which was further dropped by 5% in the next 30 days. This value is quite acceptable as compared with those highly porous polymers such as PIM-Trip-TB (CO_2 decreased 59.3% in the first 100 days),[21] KAUST-PI-1 (O_2 decreased 25% in the first 15 days),[68] PIM-PI-EA (CO_2 dropped 56% after 273 days).[20] At the same time, the CO_2/CH_4 selectivity increased from 35.6 to 44.4, and the overall separation performance was even higher than the fresh 6FPCA membrane (Fig. 7).

https://doi.org/10.1007/s10118-023-3012-5

Table 2 The *D*, *S*, of N_2, O_2, CH_4 and CO_2, and a_D, a_S of O_2/N_2 and CO_2/CH_4 for 6FPCA, 6FMCA, 6FpA, and 6FmA membranes.

Polymers		N_2	O_2	CH_4	CO_2		O_2/N_2	CO_2/CH_4
6FPCA	*P* [a]	13.6	61.5	8.99	320	*a* [d]	4.52	35.6
	D [b]	6.92	20.9	1.34	10.2	a_D [e]	3.02	7.6
	S [c]	1.97	2.95	6.73	31.3	a_S [f]	1.50	4.7
6FMCA	*P* [a]	12.8	58.8	8.75	314	*a* [d]	4.59	35.9
	D [b]	6.58	19.9	1.29	9.84	a_D [e]	3.02	7.6
	S [c]	1.95	2.95	6.79	31.9	a_S [f]	1.51	4.7
6FpA	*P* [a]	0.72	3.61	0.40	18.9	*a* [d]	5.03	47.8
	D [b]	0.60	2.38	0.16	1.07	a_D [e]	3.99	6.7
	S [c]	1.20	1.52	2.47	17.7	a_S [f]	1.27	7.2
6FmA	*P* [a]	0.34	1.63	0.17	6.49	*a* [d]	4.82	38.0
	D [b]	0.40	1.52	0.12	0.51	a_D [e]	3.85	4.3
	S [c]	0.86	1.07	1.43	12.7	a_S [f]	1.25	8.9

[a] Permeability; [b] Diffusion coefficient (10^{-8} $cm^2 \cdot s^{-1}$); [c] Solubility coefficient, (10^{-2} $cm^3 \cdot cm^{-3} \cdot cmHg^{-1}$); [d] Selectivity; [e] Diffusion selectivity; [f] Solubility selectivity.

Activation Energy of Permeation for 6FPCA and 6FpA

To study the effect of paracyclophane on the thermodynamics of gas transport in the polyimide membranes, the N_2, O_2, CH_4 and CO_2 permeability of 6FPCA and 6FpA from 30 °C to 45 °C at the interval of 5 °C of each were measured and summarized in Fig. 8 and Table S4 (in ESI). As the temperature increases, the permeability of the membrane gradually increases, whereas their permeability increment is different, *e.g.*, the N_2 permeability of 6FpA increased 45% from 30 °C to 45 °C, while in the case of 6FPCA, the N_2 only increased 16% from 13.0 Barrer to 15.1 Barrer. Compared to their decreased permeability, their O_2/N_2 and CO_2/CH_4 selectivity decrement demonstrated a reverse effect, *e.g.*, the O_2/N_2 selectivity decreased 9.2% (from 4.65 to 4.22) for 6FPCA and 19% (from 5.44 to 4.40) for 6FpA membrane. This result indicates that the 6FPCA is not sensitive to temperature change. Interestingly, there is a continuous CO_2 permeability combined with CO_2/N_2 selectivity increment simultaneously upon temperature decreasing, which has great potential in low temperature-based CO_2 separations.

The temperature dependent N_2, O_2, CH_4 and CO_2 permeability of 6FPCA and 6FpA are shown in Fig. 8. The active energy of permeation (E_p) for the above gases can be calculated by the Arrhenius-Vaṅt-Hoff equation:[69]

$$P = P_0 \exp\left(\frac{-E_p}{RT}\right) \quad (1)$$

where *R* is the ideal gas constant (1.987 $cal \cdot mol^{-1} \cdot K^{-1}$), *T* is the absolute temperature (K), *P* and P_0 are permeability at the target temperature and infilate temperatures, respectively (Barrer, 1 Barrer=10^{-10} $cm^3 \cdot cm \cdot cm^{-2} \cdot s^{-1} \cdot cmHg^{-1}$).

The correlation coefficients are over 0.999, and the E_p for 6FPCA and 6FpA, and their curves are shown in Table 3. The result turned out that the E_p sequences for different gases of 6FPCA and 6FpA are the same, that is, $CH_4 > N_2 > O_2 > CO_2$, which is the same as the dynamic diameters of the gas molecules, *i.e.*, CH_4 (3.84 Å) > N_2 (3.64 Å) > O_2 (3.46 Å) > CO_2 (3.30 Å),[48] indicating the transport is diffusion control. Additionally, the E_p of 6FpA is much larger than 6FPCA; for example, the E_p of N_2 for 6FpA and 6FPCA are 4.7 and 1.9 $kcal \cdot mol^{-1}$. This is because the 6FpA having more compact chain packing that needs more energy for gas transport. The E_p of 6FpA is comparable to those of very low permeable commercial membranes such as PC (Table 3). Interestingly, the E_p of 6FPCA for all gases significantly decreased to even lower than that of highly porous PIM-1, probably due to the introduction of paracyclophane subunit creating some extra pathway to transport gas molecules. However, detailed reasons still need further study.

Pressure-dependent Pure- and Mixed-gas CO_2/CH_4 Separation Properties of the Membranes

In real conditions, CO_2 removal from natural gas generally happens at relatively high CO_2 partial pressure. To evaluate the

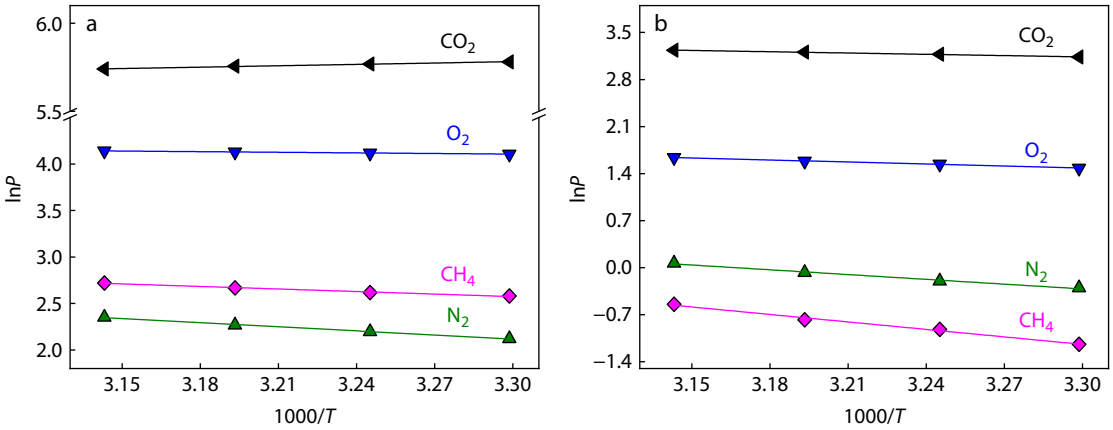

Fig. 8 Temperature dependent of permeability of N_2, O_2, CH_4 and CO_2 for (a) 6FPCA and (b) 6FpA.

https://doi.org/10.1007/s10118-023-3012-5

Table 3 E_p for 6FPCA, 6FpA and some other polymer membranes.[a]

Polymers	N_2	O_2	CH_4	CO_2
6FPCA	1.9	0.7	2.9	–0.6
6FpA	4.7	2.0	7.4	1.2
PC [b]	6.0	5.0	6.2	3.0
PIM-1 [c]	2.8	0.6	4.2	0.4

[a] Activation energy of gas permeation to the polymer membranes (kcal·mol^{-1}); [b, c] Data from references.[70,71]

real application potential of 6FPCA and 6FpA membranes, their pressure dependent separation properties of CO_2 and CH_4 were carried out and shown in Table S5 (in ESI) and Fig. 9. Both 6FPCA and 6FpA show a good plasticization resistance, as indicated by their permeability of CO_2 and CH_4 decrease as the upstream pressure increase, *i.e.*, the CO_2 permeability of 6FPCA decreased from 320 Barrer to 281 Barrer when the pressure increased from 0.2 MPa to 1.8 MPa, which is similar to the 16% decline of 6FpA membrane.

We also tested the variable pressure CO_2/CH_4 (50/50) mixed-gas separation properties of 6FPCA to evaluate its separation properties similar to real conditions (Table S6 in ESI and Fig. 10). The results show that the CO_2 permeability of 6FPCA is a slightly lower than its pure gas, *i.e.*, the permeability of CO_2 decreases from 320 Barrer of pure gas to 290 Barrer of CO_2/CH_4 (50/50) mixed-gas. This is because the competitive sorption resulted in some micropores of the membrane being occupied by CH_4 molecules and decreased the sorption of CO_2. Additionally, when the mixed-gas pressure went up from 0.2 MPa to 2.0 MPa, there was still no plasticization proved by the continuously decrease of CO_2 and CH_4 permeability. However, even under the upstream mixed-gas pressure of 2.0 MPa, the CO_2 permeability still reach as much as 201 Barrer and CO_2/CH_4 selectivity of 34. This value is still above the 2018 mixed-gas CO_2/CH_4 trade-off line (Fig. 10b), which provides great potential in membrane-based CO_2 removal from natural gas.

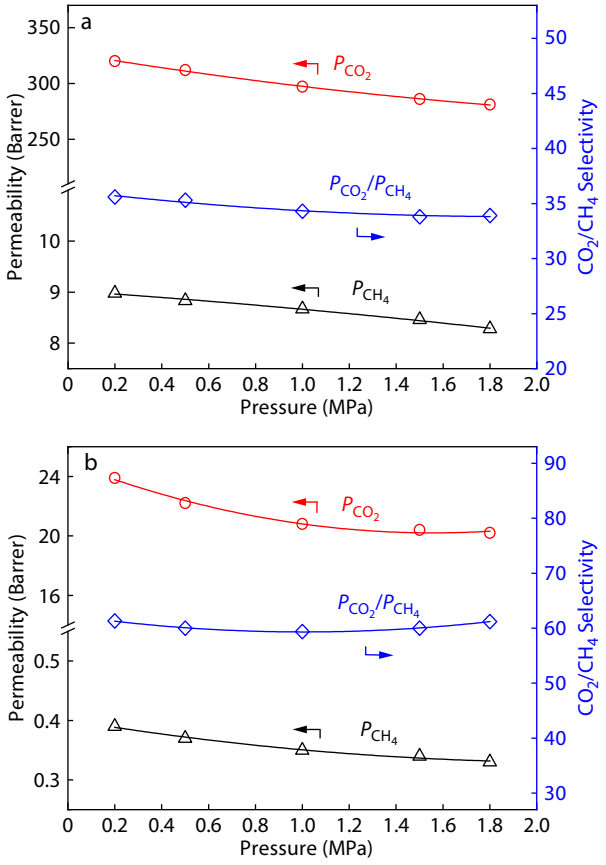

Fig. 9 Pressure-dependent gas separation properties of (a) 6FPCA and (b) 6FpA for CH_4 and CO_2.

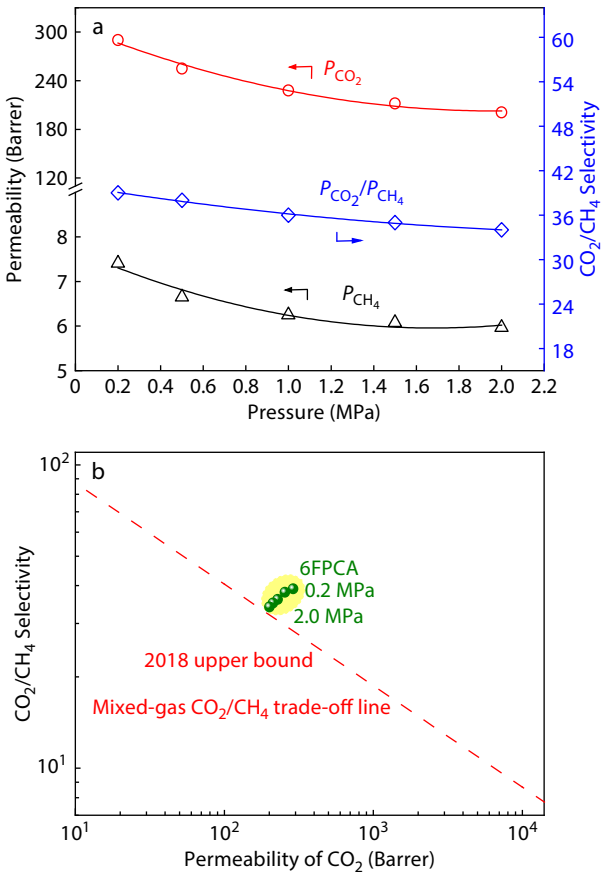

Fig. 10 (a) Pressure-dependent CO_2/CH_4 mixed-gas separation performance of 6FPCA; (b) The CO_2/CH_4 mixed-gas separation performance for 6FPCA. The 2018 mixed-gas CO_2/CH_4 Upper Bound line is from Ref. [72].

CONCLUSIONS

We synthesized two diamine regioisomers based on paracyclophane as the site of contortion by Pd catalyst C—N coupling reaction, and used them as monomers for the synthesis of intrinsic microporous polyimides 6FPCA and 6FMCA for the first time. The chemical structure of the monomers, and polyimides was carefully analyzed and proved by their NMR, FT-IR, and elementary analysis. These two PIM-PIs demonstrate good solubility, excellent thermal stability with onset decomposition temperature of ~508 °C, and mechanical strength. Compared with the plane structure of 6FpA and 6FmA, the 6FPCA and 6FPMA exhibited a significantly increased microporosity (420–434 m^2·g^{-1} versus 97–120 m^2·g^{-1}), FFV (0.22 versus 0.15) and enlarged the *d*-spacing (6.5–6.9 Å versus

https://doi.org/10.1007/s10118-023-3012-5

5.6–5.9 Å) of the polymer main chains. The gas permeability results indicated that the 6FPCA and 6FMCA had over 10 times higher permeability than their corresponding 6FpA and 6FmA membranes without loose selectivity too much, which hugely increased the separation performance of the 6FPCA and 6FMCA from far below to close the 2008 Robeson upper bound. At the same time, the 6FPCA also demonstrates good plasticization resistance, moderate aging properties, and CO_2/CH_4 mixed-gas separation performance. Considering the significant improvement in their gas separation properties after introducing the paracyclophane subunit into the polymers, it provides a great perspective in tailoring the desired properties of intrinsic microporous polymers for various applications by adopting the topological micropores.

Conflict of Interests

The authors declare no interest conflict.

Electronic Supplementary Information

Electronic supplementary information (ESI) is available free of charge in the online version of this article at http://doi.org/10.1007/s10118-023-3012-5.

ACKNOWLEDGMENTS

This work was financially supported by the National Natural Science Foundation of China (Nos. 22078245 and 21861016), YLU-DNL Fund (No. 2022009). We also greatly appreciate the characterization by the Analytic and Testing Center of Tiangong University.

REFERENCES

1 Sholl, D. S.; Lively, R. P. Seven chemical separations to change the world. *Nature* **2016**, *532*, 435–437.
2 Galizia, M.; Chi, W. S.; Smith, Z. P.; Merkel, T. C.; Baker, R. W.; Freeman, B. D. 50th Anniversary perspective: polymers and mixed matrix membranes for gas and vapor separation: a review and prospective opportunities. *Macromolecules* **2017**, *50*, 7809–7843.
3 Sandru, M.; Sandru, E. M.; Ingram, W. F.; Deng, J.; Stenstad, P. M.; Deng, L.; Spontak, R. J. An integrated materials approach to ultrapermeable and ultraselective CO_2 polymer membranes. *Science* **2022**, *376*, 90–94.
4 Park, H. B.; Kamcev, J.; Robeson, L. M.; Elimelech, M.; Freeman, B. D. Maximizing the right stuff: the trade-off between membrane permeability and selectivity. *Science* **2017**, *356*, eaab0530.
5 Zhu, B.; He, S.; Yang, Y.;Li, S.; Lau, C. H.; Liu, S.; Shao, L. Boosting membrane carbon capture *via* multifaceted polyphenol-mediated soldering. *Nat. Commun.* **2023**, *14*, 1697.
6 Zhu, B.; He, S.; Wu, Y.; Li, S.; Shao, L. One-step synthesis of structurally stable CO_2-philic membranes with ultra-high PEO loading for enhanced carbon capture. *Engineering* **2022**, doi: 10.1016/j.eng.2022.03.016.
7 Robeson, L. M. The upper bound revisited. *J. Membr. Sci.* **2008**, *320*, 390–400.
8 Swaidan, R.; Ghanem, B.; Pinnau, I. Fine-tuned intrinsically ultramicroporous polymers redefine the permeability/selectivity upper bounds of membrane-based air and hydrogen separations. *ACS Macro Lett.* **2015**, *4*, 947–951.
9 Freeman, B. D. Basis of permeability/selectivity tradeoff relations in polymeric gas separation membranes. *Macromolecules* **1999**, *32*, 375–380.
10 Comesaña-Gándara, B.; Chen, J.; Bezzu, C. G.; Carta, M.; Rose, I.; Ferrari, M. C.; Esposito, E.; Fuoco, A.; Jansen, J. C.; McKeown, N. B. Redefining the Robeson upper bounds for CO_2/CH_4 and CO_2/N_2 separations using a series of ultrapermeable benzotriptycene-based polymers of intrinsic microporosity. *Energy Environ. Sci.* **2019**, *12*, 2733–2740.
11 Du, N.; Park, H. B.; Robertson, G. P.; Dal-Cin, M. M.; Visser, T.; Scoles, L.; Guiver, M. D. Polymer nanosieve membranes for CO_2-capture applications. *Nat. Mater.* **2011**, *10*, 372–375.
12 Yin, Y.; Guiver, M. D. Microporous polymers: ultrapermeable membranes. *Nat. Mater.* **2017**, *16*, 880–881.
13 Guiver, M. D.; Lee, Y. M. Polymer rigidity improves microporous membranes. *Science* **2013**, *339*, 284–285.
14 Budd, P. M.; Ghanem, B. S.; Makhseed, S.; McKeown, N. B.; Msayib, K. J.; Tattershall, C. E. Polymers of intrinsic microporosity (PIMs): robust, solution-processable, organic nanoporous materials. *Chem. Commun.* **2004**, 230–231.
15 Budd, P. M.; McKeown, N. B.; Fritsch, D. Free volume and intrinsic microporosity in polymers. *J. Mater. Chem.* **2005**, *15*, 1977–1986.
16 Budd, P. M.; Msayib, K. J.; Tattershall, C. E.; Ghanem, B. S.; Reynolds, K. J.; McKeown, N. B.; Fritsch, D. Gas separation membranes from polymers of intrinsic microporosity. *J. Membr. Sci.* **2005**, *251*, 263–269.
17 Li, P.; Chung, T. S.; Paul, D. R. Gas sorption and permeation in PIM-1. *J. Membr. Sci.* **2013**, *432*, 50–57.
18 Ghanem, B. S.; McKeown, N. B.; Budd, P. M.; Selbie, J. D.; Fritsch, D. High-performance membranes from polyimides with intrinsic microporosity. *Adv. Mater.* **2008**, *20*, 2766–2771.
19 Bezzu, C. G.; Carta, M.; Tonkins, A.; Jansen, J. C.; Bernardo, P.; Bazzarelli, F.; McKeown, N. B. A spirobifluorene-based polymer of intrinsic microporosity with improved performance for gas separation. *Adv. Mater.* **2012**, *24*, 5930–5933.
20 Carta, M.; Malpass-Evans, R.; Croad, M.; Rogan, Y.; Jansen, J. C.; Bernardo, P.; Bazzarelli, F.; McKeown, N. B. An efficient polymer molecular sieve for membrane gas separations. *Science* **2013**, *339*, 303–307.
21 Carta, M.; Croad, M.; Malpass-Evans, R.; Jansen, J. C.; Bernardo, P.; Clarizia, G.; Friess, K.; Lanc, M.; McKeown, N. B. Triptycene induced enhancement of membrane gas selectivity for microporous Troger's base polymers. *Adv. Mater.* **2014**, *26*, 3526–3531.
22 Rose, I.; Bezzu, C. G.; Carta, M.; Comesana-Gandara, B.; Lasseuguette, E.; Ferrari, M. C.; Bernardo, P.; Clarizia, G.; Fuoco, A.; Jansen, J. C.; Hart, K. E.; Liyana-Arachchi, T. P.; Colina, C. M.; McKeown, N. B. Polymer ultrapermeability from the inefficient packing of 2D chains. *Nat. Mater.* **2017**, *16*, 932–937.
23 Lai, H. W. H.; Benedetti, F. M.; Ahn, J. M.; Robinson, A. M.; Wang, Y.; Pinnau, I.; Smith, Z. P.; Xia, Y. Hydrocarbon ladder polymers with ultrahigh permselectivity for membrane gas separations. *Science* **2022**, *375*, 1390–1392.
24 Budd, P. M.; Elabas, E. S.; Ghanem, B. S.; Makhseed, S.; McKeown, N. B.; Msayib, K. J.; Tattershall, C. E.; Wang, D. Solution-processed, organophilic membrane derived from a polymer of intrinsic microporosity. *Adv. Mater.* **2004**, *16*, 456–459.
25 Yi, S.; Ghanem, B.; Liu, Y.; Pinnau, I.; Koros, W. J. Ultraselective glassy polymer membranes with unprecedented performance for energy-efficient sour gas separation. *Sci. Adv.* **2019**, *5*, eaaw5459.
26 Ma, X.; Lai, H. W. H.; Wang, Y.; Alhazmi, A.; Xia, Y.; Pinnau, I. Facile synthesis and study of microporous catalytic arene-norbornene annulation-Tröger's base ladder polymers for membrane air separation. *ACS Macro Lett.* **2020**, *9*, 680–685.

27 Ma, X. H.; Abdulhamid, M. A.; Pinnau, I. Design and synthesis of polyimides based on carbocyclic pseudo-Troger's base-derived dianhydrides for membrane gas separation applications. *Macromolecules* **2017**, *50*, 5850–5857.
28 Ma, X. H.; Ghanem, B.; Salinas, O.; Litwiller, E.; Pinnau, I. Synthesis and effect of physical aging on gas transport properties of a microporous polyimide derived from a novel spirobifluorene-based dianhydride. *ACS Macro Lett.* **2015**, *4*, 231–235.
29 Ma, X. H.; Salinas, O.; Litwiller, E.; Pinnau, I. Novel spirobifluorene- and dibromospirobifluorene-based polyimides of intrinsic microporosity for gas separation applications. *Macromolecules* **2013**, *46*, 9618–9624.
30 Ghanem, B. S.; Swaidan, R.; Litwiller, E.; Pinnau, I. Ultra-Microporous triptycene-based polyimide membranes for high-performance gas separation. *Adv. Mater.* **2014**, *26*, 3688–3692.
31 Ghanem, B. S.; Swaidan, R.; Ma, X.; Litwiller, E.; Pinnau, I. Energy-efficient hydrogen separation by AB-type ladder-polymer molecular sieves. *Adv. Mater.* **2014**, *26*, 6696–6700.
32 Bezzu, C. G.; Fuoco, A.; Esposito, E.; Monteleone, M.; Longo, M.; Jansen, J. C.; Nichol, G. S.; McKeown, N. B. Ultrapermeable polymers of intrinsic microporosity containing spirocyclic units with fused triptycenes. *Adv. Funct. Mater.* **2021**, *31*, 2104474.
33 Williams, R.; Burt, L. A.; Esposito, E.; Jansen, J. C.; Tocci, E.; Rizzuto, C.; Lanc, M.; Carta, M.; McKeown, N. B. A highly rigid and gas selective methanopentacene-based polymer of intrinsic microporosity derived from Troger's base polymerization. *J. Mater. Chem. A* **2018**, *6*, 5661–5667.
34 Rose, I.; Carta, M.; Malpass-Evans, R.; Ferrari, M. C.; Bernardo, P.; Clarizia, G.; Jansen, J. C.; McKeown, N. B. Highly permeable benzotriptycene-based polymer of intrinsic microporosity. *ACS Macro Lett.* **2015**, *4*, 912–915.
35 Liu, J.; Xiao, Y.; Liao, K. S.; Chung, T. S. Highly permeable and aging resistant 3D architecture from polymers of intrinsic microporosity incorporated with beta-cyclodextrin. *J. Membr. Sci.* **2017**, *523*, 92–102.
36 Liang, C. Z.; Liu, J. T.; Lai, J. Y.; Chung, T. S. High-performance multiple-layer PIM composite hollow fiber membranes for gas separation. *J. Membr. Sci.* **2018**, *563*, 93–106.
37 Villalobos, L. F.; Huang, T.; Peinemann, K. V. Cyclodextrin films with fast solvent transport and shape-selective permeability. *Adv. Mater.* **2017**, *29*, 1606641.
38 Liu, J.; Hua, D.; Zhang, Y.; Japip, S.; Chung, T. S. Precise molecular sieving architectures with Janus pathways for both polar and nonpolar molecules. *Adv. Mater.* **2018**, *30*, 1705933.
39 Huang, T.; Puspasari, T.; Nunes, S. P.; Peinemann, K. V. Ultrathin 2D-layered cyclodextrin membranes for high-performance organic solvent nanofiltration. *Adv. Funct. Mater.* **2019**, *30*, 1906797.
40 Huang, T.; Moosa, B. A.; Hoang, P.; Liu, J.; Chisca, S.; Zhang, G.; AlYami, M.; Khashab, N. M.; Nunes, S. P. Molecularly-porous ultrathin membranes for highly selective organic solvent nanofiltration. *Nat. Commun.* **2020**, *11*, 5882.
41 Li, B.; Japip, S.; Chung, T. S. Molecularly tunable thin-film nanocomposite membranes with enhanced molecular sieving for organic solvent forward osmosis. *Nat. Commun.* **2020**, *11*, 1198.
42 Jiang, Z.; Dong, R.; Evans, A. M.; Biere, N.; Ebrahim, M. A.; Li, S.; Anselmetti, D.; Dichtel, W. R.; Livingston, A. G. Aligned macrocycle pores in ultrathin films for accurate molecular sieving. *Nature* **2022**, *609*, 58–64.
43 Cram, D. J.; Steinberg, H. Macro Rings. I. Preparation and spectra of the paracyclophanes. *J. Am. Chem. Soc.* **1951**, *73*, 5691–5704.
44 Hassan, Z.; Spuling, E.; Knoll, D. M.; Brase, S. Regioselective functionalization of [2.2]paracyclophanes: recent synthetic progress and perspectives. *Angew. Chem. Int. Ed.* **2020**, *59*, 2156–2170.
45 Hassan, Z.; Varadharajan, D.; Zippel, C.; Begum, S.; Lahann, J.; Brase, S. Design strategies for structurally controlled polymer surfaces *via* cyclophane-based CVD polymerization and post-CVD fabrication. *Adv. Mater.* **2022**, *34*, e2201761.
46 Kumar, S. V.; Guiry, P. J. Zinc-catalyzed enantioselective [3+2] cycloaddition of azomethine ylides using planar chiral [2.2]paracyclophane-imidazoline N,O-ligands. *Angew. Chem. Int. Ed.* **2022**, *61*, e202205516.
47 Liao, X. J.; Pu, D.; Yuan, L.; Tong, J.; Xing, S.; Tu, Z. L.; Zuo, J. L.; Zheng, W. H.; Zheng, Y. X. Planar chiral multiple resonance thermally activated delayed fluorescence materials for efficient circularly polarized electroluminescence. *Angew. Chem. Int. Ed.* **2023**, *62*, e202217045.
48 Pye, D. G.; Hoehn, H. H.; Panar, M. Measurement of gas permeability of polymers. I. Permeabilities in constant volume/variable pressure apparatus. *J. Appl. Polym. Sci.* **1976**, *20*, 1921–1931.
49 Ye, C.; Luo, C.; Ji, W.; Weng, Y.; Li, J.; Yi, S.; Ma, X. Significantly enhanced gas separation properties of microporous membranes by precisely tailoring their ultra-microporosity through bromination/debromination. *Chem. Eng. J.* **2023**, *451*, 138513.
50 Yeh, Y. L.; Gorham, W. F. Preparation and reactions of some [2.2] paracyclophane derivatives. *J. Org. Chem.* **2002**, *34*, 2366–2370.
51 Ruiz-Castillo, P.; Buchwald, S. L. Applications of palladium-catalyzed C-N cross-coupling reactions. *Chem. Rev.* **2016**, *116*, 12564–12649.
52 Snyder, R. W.; Thomson, B.; Bartges, B.; Czerniawski, D.; Painter, P. C. FTIR studies of polyimides: thermal curing. *Macromolecules* **2002**, *22*, 4166–4172.
53 Mi, Y.; Stern, S. A.; Trohalaki, S. Dependence of the gas-permeability of some polyimide isomers on their intrasegmental mobility. *J. Membr. Sci.* **1993**, *77*, 41–48.
54 McKeown, N. B.; Budd, P. M. Polymers of intrinsic microporosity (PIMs): organic materials for membrane separations, heterogeneous catalysis and hydrogen storage. *Chem. Soc. Rev.* **2006**, *35*, 675–683.
55 Alghunaimi, F.; Ghanem, B.; Alaslai, N.; Swaidan, R.; Litwiller, E.; Pinnau, I. Gas permeation and physical aging properties of iptycene diamine-based microporous polyimides. *J. Membr. Sci.* **2015**, *490*, 321–327.
56 Li, K.; Zhu, Z.; Dong, H.; Li, Q.; Ji, W.; Li, J.; Cheng, B.; Ma, X. Bottom up approach to study the gas separation properties of PIM-PIs and its derived CMSMs by isomer monomers. *J. Membr. Sci.* **2021**, *635*, 119519.
57 Ma, X. H.; Swaidan, R.; Belmabkhout, Y.; Zhu, Y. H.; Litwiller, E.; Jouiad, M.; Pinnau, I.; Han, Y. Synthesis and gas transport properties of hydroxyl-functionalized polyimides with intrinsic microporosity. *Macromolecules* **2012**, *45*, 3841–3849.
58 Bondi, A. van der Waals volumes and radii. *J. Phys. Chem.* **1964**, *68*, 441–451.
59 Nuhnen, A.; Klopotowski, M.; Tanh Jeazet, H. B.; Sorribas, S.; Zornoza, B.; Tellez, C.; Coronas, J.; Janiak, C. High performance MIL-101(Cr)@6FDA-mPD and MOF-199@6FDA-mPD mixed-matrix membranes for CO_2/CH_4 separation. *Dalton Trans.* **2020**, *49*, 1822–1829.
60 Alaslai, N.; Ghanem, B.; Alghunaimi, F.; Litwiller, E.; Pinnau, I. Pure- and mixed-gas permeation properties of highly selective and plasticization resistant hydroxyl-diamine-based 6FDA polyimides for CO_2/CH_4 separation. *J. Membr. Sci.* **2016**, *505*, 100–107.
61 Ma, X. H.; Salinas, O.; Litwiller, E.; Pinnau, I. Pristine and thermally-rearranged gas separation membranes from novel *o*-hydroxyl-functionalized spirobifluorene-based polyimides. *Polym. Chem.* **2014**, *5*, 6914–6922.
62 Swaidan, R.; Ghanem, B.; Litwiller, E.; Pinnau, I. Effects of hydroxyl-

functionalization and sub-T_g thermal annealing on high pressure pure- and mixed-gas CO_2/CH_4 separation by polyimide membranes based on 6FDA and triptycene-containing dianhydrides. *J. Membr. Sci.* **2015**, *475*, 571–581.
63 Jung, C. H.; Lee, Y. M. Gas permeation properties of hydroxyl-group containing polyimide membranes. *Macromol. Res.* **2008**, *16*, 555–560.
64 Coleman, M. R.; Koros, W. J. Isomeric polyimides based on fluorinated dianhydrides and diamines for gas separation applications. *J. Membr. Sci.* **1990**, *50*, 285–297.
65 Alaslai, N.; Ma, X.; Ghanem, B.; Wang, Y.; Alghunaimi, F.; Pinnau, I. Synthesis and characterization of a novel microporous dihydroxyl-functionalized triptycene-diamine-based polyimide for natural gas membrane separation. *Macromol. Rapid Commun.* **2017**, *38*, 1700303.
66 Low, Z. X.; Budd, P. M.; McKeown, N. B.; Patterson, D. A. Gas permeation properties, physical aging, and its mitigation in high free volume glassy polymers. *Chem. Rev.* **2018**, *118*, 5871–5911.
67 Lau, C. H.; Mulet, X.; Konstas, K.; Doherty, C. M.; Sani, M. A.; Separovic, F.; Hill, M. R.; Wood, C. D. Hypercrosslinked additives for ageless gas-separation membranes. *Angew. Chem. Int. Ed.* **2016**, *55*, 1998–2001.
68 Swaidan, R.; Ghanem, B.; Litwiller, E.; Pinnau, I. Physical aging, plasticization and their effects on gas permeation in "rigid" polymers of intrinsic microporosity. *Macromolecules* **2015**, *48*, 6553–6561.
69 Costello, L. M.; Koros, W. J. Effect of structure on the temperature dependence of gas transport and sorption in a series of polycarbonates. *J. Polym. Sci., Part B: Polym. Phys.* **1994**, *32*, 701–713.
70 Muruganandam, N.; Koros, W. J.; Paul, D. R. Gas sorption and transport in substituted polycarbonates. *J. Polym. Sci., Part B: Polym. Phys.* **1987**, *25*, 1999–2026.
71 Li, P.; Chung, T. S.; Paul, D. R. Temperature dependence of gas sorption and permeation in PIM-1. *J. Membr. Sci.* **2014**, *450*, 380–388.
72 Wang, Y.; Ma, X.; Ghanem, B. S.; Alghunaimi, F.; Pinnau, I.; Han, Y. Polymers of intrinsic microporosity for energy-intensive membrane-based gas separations. *Mater. Today Nano* **2018**, *3*, 69–95.

https://doi.org/10.1007/s10118-023-3012-5